CYBERNETICS AND PHYSICS, VOL. 1, NO. 1, 2012 , 42–50

REDUCED NORMAL FORM APPROACH TO SWING CONTROL OF CRANE SYSTEMS: THEORY AND EXPERIMENTS

Edwin Kreuzer
Institute of Mechanics and Ocean Engineering
Hamburg University of Technology
Germany
kreuzer@tu-harburg.de

N. Sri Namachchivaya
Department of Aerospace Engineering
University of Illinois at Urbana-Champaign
Illinois, USA
navam@illinois.edu

Marc-André Pick
Institute of Mechanics and Ocean Engineering
Hamburg University of Technology
Germany
pick@tu-harburg.de

Christian Rapp
Institute of Mechanics and Ocean Engineering
Hamburg University of Technology
Germany
christian.rapp@tu-harburg.de

Abstract
Load oscillations of container cranes reduce the container handling throughput and need to be controlled in order to minimize load swing. The proposed controller is motivated by a novel reduced normal form technique that incorporates resonant coupling into the underactuated system of load oscillations and hoisting mechanism. Results from simulations prove the functionality of the controller and motivate its implementation at the container crane test stand.

Key words
Reduced normal form, container crane, swing control, oscillations, resonant coupling controller.

1 Introduction

In 2009 the containerization (transported goods in standardized containers throughout the world) has reached a value of almost 97%. This number indicates that nearly all transported goods have to be handled at least two times by container cranes, if they are shipped by sea route. This huge amount of goods carried by container vessels on long distance routes, e.g. from Asia to North America or to Europe gives many reasons for increasing the efficiency of the transportation process.

During the last decades the vessels became larger and wider and were able to carry more containers per cruise. The first container vessel in the world for shipping ISO–containers was the *Ideal–X* operated by the *Sea–Land Corporation* with a capacity of 58 TEU (twenty foot equivalent units) in 1956. Today the largest vessels (*Emma–Maersk*–class) have a capacity of 15,500 TEU, vessels with a capacity of 18,000 TEU were ordered by the Maersk Line in 2011. An end of this development is not predictable at the present time.

1.1 Container cranes

The increase of the efficiency by using longer and wider vessels to carry more containers per cruise leads to a loss of efficiency during the loading and unloading procedure at the port. The dimensions of the container cranes grew with the growth of the vessels. A sketch of a modern container crane that is used at the Port of Hamburg at the Altenwerder Terminal is shown in Fig. 1. This provides a waterside outreach of about $D_{ws} = 61$m for vessels, which can be can be handled by, for example, *Emma Maersk*. The maximum hoisting distance is $H_1 = 62$m, with a distance of $H_2 = 39$m above the water line. When transporting a container from the quay–side to its designated position on the vessel an increase of trolley traveling distance automatically extends the duration of container handling. Faster movements with higher acceleration rates of the trolley favor the occurrence of load oscillations. Thus, the extended trolley traveling distance and load oscillations decrease the number of container moves per hour at the port. Simultaneously, it reduces the ship loading (unloading) efficiency and increases berth cost.

During the last decades, a lot of effort has been put into reducing load swing by controlling the motion of the container crane trolley. A broad overview of current trolley control schemes is given by [Abdel-Rahman et al., 2003]. It was pointed out that only load swing in

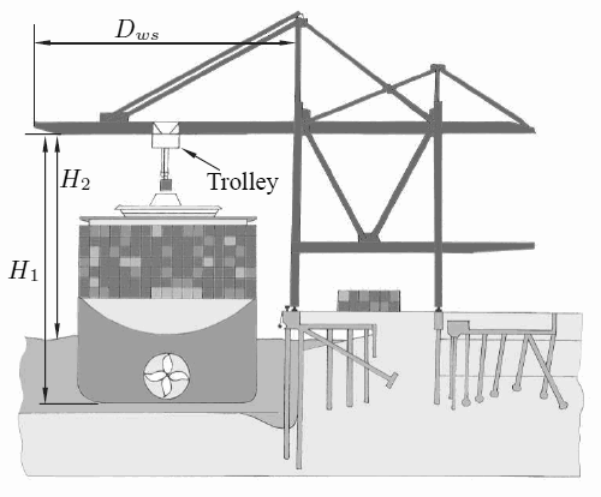

Figure 1. Sketch of the container crane in operation.

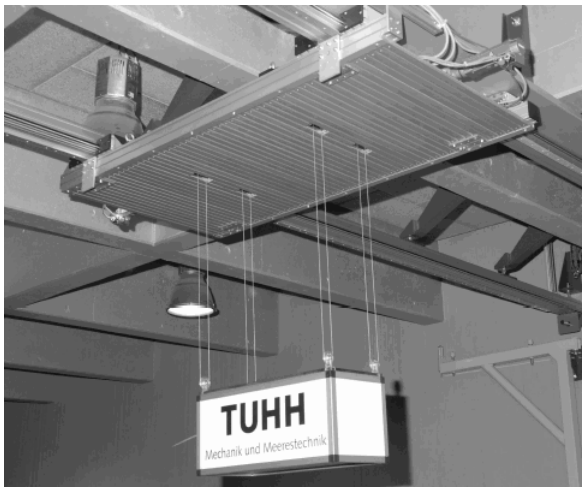

Figure 2. Container crane test stand.

the plane of the trolley direction and the gravitational axis can be suppressed with the control input, while the rotational motions of the load or load swing in the plane perpendicular to the trolley direction cannot be affected by trolley motions. Moreover, every motion of the trolley effects the crane operator whos cabin is mounted on the trolley.

In order to overcome these disadvantages this paper proposes a novel normal form approach focusing on internal resonances of the hoisting mechanism and the load swing. No control input to the trolley is required to reduce spatial load swing. After this introduction we start by stating a brief description of the normal form representation of a given system, followed by the reduced normal form, which is the basis of the resonant coupling controller.

1.2 Container crane test stand

The developed control scheme will be implemented, applied and validated by experiments with the container crane test stand at the Institute of Mechanics and Ocean Engineering of Hamburg University of Technology. The test was designed to create an experimental base for various research topics on dynamics and control theory of mechatronic systems. The test stand, shown in Fig. 2 was built in 2009 and is mounted directly below the concrete ceiling construction to fit the laboratory's dimensions. The hoisting height is about 11m and the trolley traveling distance is about 13m with a length of the tracks of 15m. Compared to a container crane described earlier and shown in Fig. 1 with a land- and seaside trolley traveling distance of about 80m and a maximum hoisting height of 65m the test stand is designed at a scale of approximately 1:6. The presented results within the experimental validation section were completely taken at the container crane test stand.

1.3 Normal forms

The system under consideration, container crane load swing, is represented as an autonomous nonlinear control system in the form

$$\dot{x}(t) = b(x(t)) + \sigma(x(t))u(t), \tag{1}$$

where $x \in \mathbb{R}^n$, $u \in \mathbb{R}^{n_c}$, b, and σ are real analytic functions. Using a Taylor series this formulation becomes linear in $\tilde{F}$ and $\tilde{G}$ plus remaining nonlinear parts $\hat{b}(x)$ and $\hat{\sigma}(x)u$:

$$\dot{x} = \tilde{F}x + \tilde{G}u + \hat{b}(x) + \hat{\sigma}(x)u. \tag{2}$$

A near-identity change of coordinates $\Phi(y)$ transforms the original system (2) into normal form representation (refer to [Arnold, 1983] for further details)

$$x = \Phi(y) = y + \Phi^{[2]}(y) + \Phi^{[3]}(y) + \ldots, \tag{3}$$
$$\dot{y} = Fy + Gu + \mathfrak{b}(y) + \bar{\sigma}(y)v, \tag{4}$$

which only contains normal form nonlinear parts $\mathfrak{b}(y)$ of the transformed system. Other nonlinearities have been erased by the transformation (3). The superscript refers to the order $O(k)$ of the corresponding nonlinear term. The input states as

$$u = \alpha^{[k]}(y) + \beta^{[k-1]}(y)v + v. \tag{5}$$

Two homological equations (see [Krener and Kang, 1990] and [Talwar and Namachchivaya, 1992]) can be found from the transformation (3) together with (2) to derive the transformation $\Phi^{[k]}(y)$ itself, the normal forms $\mathfrak{b}^{[k]}(y)$, control terms $\bar{\sigma}^{[k-1]}(y)$, and input parameters $\alpha^{[k]}(y)$, $\beta^{[k-1]}(y)$ up to order k.

Similar investigations have been carried out by [Khajepour and Golnaraghi, 1994], [Khajepour et al., 1997]

and [Krener et al., 2001] focusing on the classical normal form of similar systems. It requires a large amount of calculations even for low order systems. In the following section a method with reduced cost of calculation is outlined with the aim to identify the governing nonlinearities.

2 Reduced normal forms

Decomposing the original state $x \stackrel{\text{def}}{=} (x_u,\, x_c)^T$ into uncontrollable $x_u \in \mathbb{R}^{n_u}$ and controllable variables $x_c \in \mathbb{R}^{n_c}$ leads to the new system based on (2)

$$\begin{pmatrix} \dot{x}_u \\ \dot{x}_c \end{pmatrix} = \underbrace{\begin{bmatrix} \tilde{A} & 0 \\ 0 & \tilde{C} \end{bmatrix}}_{\tilde{F}} \begin{pmatrix} x_u \\ x_c \end{pmatrix} + \underbrace{\begin{bmatrix} 0 \\ \tilde{B} \end{bmatrix}}_{\tilde{G}} u + + \underbrace{\begin{pmatrix} f(x_u, x_c) \\ g(x_u, x_c) \end{pmatrix}}_{\hat{b}} + \underbrace{\begin{pmatrix} \nu(x_u, x_c) \\ \mu(x_u, x_c) \end{pmatrix}}_{\hat{\sigma}} u. \quad (6)$$

Transformation (3) is decoupled in a similar manner, taking into account uncontrollable normal form modes $\xi \in \mathbb{C}^{n_u}$ and controllable normal form modes $\eta \in \mathbb{C}^{n_c}$. Notice the change from real to complex notation $x \to z \in \mathbb{C}^k$ and further to normal form notation $z = \Phi(y)$, $y = (\xi, \bar{\xi}, \eta, \bar{\eta})^T \in \mathbb{C}^k$. This benefits in less system equations due to the complex conjugate equations. It now states $z = y + \left(h^{[k]}(y),\, \varphi^{[k]}(y)\right)^T$ and together with the homological equations from [Talwar and Namachchivaya, 1992] and (6) one derives

$$\begin{aligned} \mathfrak{f}^{[k]}(\xi,\eta) = {} & Ah^{[k]}(\xi,\eta) - \frac{\partial h^{[k]}}{\partial \xi}(\xi,\eta)A\xi \\ & - \frac{\partial h^{[k]}}{\partial \eta}(\xi,\eta)C\eta + f^{[k]}(\xi,\eta), \quad (7) \end{aligned}$$

$$\begin{aligned} \mathfrak{g}^{[k]}(\xi,\eta) = {} & C\varphi^{[k]}(\xi,\eta) - \frac{\partial \varphi^{[k]}}{\partial \xi}(\xi,\eta)A\xi \\ & - \frac{\partial \varphi^{[k]}}{\partial \eta}(\xi,\eta)C\eta + g^{[k]}(\xi,\eta) \\ & + B\alpha^{[k]}(\xi,\eta), \quad (8) \end{aligned}$$

$$\begin{aligned} \bar{\nu}^{[k-1]}(\xi,\eta)v = {} & -\frac{\partial h^{[k]}}{\partial \eta}(\xi,\eta)Bv \\ & + \nu^{[k-1]}(\xi,\eta)v, \quad (9) \end{aligned}$$

$$\begin{aligned} \bar{\mu}^{[k-1]}(\xi,\eta)v = {} & -\frac{\partial \varphi^{[k]}}{\partial \eta}(\xi,\eta)B\,v \\ & + B\beta^{[k-1]}(\xi,\eta)v \\ & + \mu^{[k-1]}(\xi,\eta)v. \quad (10) \end{aligned}$$

A further decomposition of the k-th order nonlinear terms of the transformation into monomials of uncontrollable, controllable and mixed modes ($|m| + |l| = k$, $\varphi^{[k]}$ likewise) is employed:

$$\begin{aligned} h^{[k]}(\xi,\eta) = {} & h^{(m,0)}(\xi) + h^{(m,l)}(\xi,\eta) \\ & + h^{(0,l)}(\eta), \quad (11) \end{aligned}$$

with

$$h^{(m,l)}(\xi,\eta) \stackrel{\text{def}}{=} \sum_k \sum_i h^{(m,l)}_{i:m_1\ldots m_{n_u} l_1 \ldots l_{n_u}} \xi_1^{m_1} \cdots \ldots \xi_{n_u}^{m_{n_u}} \eta_1^{l_1} \ldots \eta_{n_c}^{l_{n_c}} \mathbf{e}_i.$$

Inserting the decomposed transformation (11) into (7) through (10) yields for $k = 2$ ten equations. Out of these ten equations (equivalent to classical normal form derivation) e.g. only three have to be taken into account when deriving the reduced normal form of the planar elastic pendulum (representing the underactuated system):

$$\begin{aligned} & \frac{\partial \varphi^{(2,0)}}{\partial \xi}(\xi)A\xi - C\varphi^{(2,0)}(\xi) - B\alpha^{(2,0)}(\xi) \\ & \qquad = g^{(2,0)}(\xi) - \mathfrak{g}^{(2,0)}(\xi), \quad (12) \end{aligned}$$

$$\begin{aligned} & \frac{\partial h^{(1,1)}}{\partial \xi}(\xi,\eta)A\xi + \frac{\partial h^{(1,1)}}{\partial \eta}(\xi,\eta)C\eta \\ & -Ah^{(1,1)}(\xi,\eta) = f^{(1,1)}(\xi,\eta) - \mathfrak{f}^{(1,1)}(\xi,\eta), \quad (13) \end{aligned}$$

$$\frac{\partial h^{(1,1)}}{\partial \eta}(\xi,\eta)B = \nu^{(1,0)}(\xi) - \bar{\nu}^{(1,0)}(\xi). \quad (14)$$

Based on the given system (6) the remaining conditions (12) through (14) are solved for the normal form nonlinearities $\mathfrak{g}^{[k]}$ and $\mathfrak{f}^{[k]}$, the near-identity terms $h^{[k]}$ and $\varphi^{[k]}$ as well as the control parameter $\alpha^{[k]}$. The normal form of each subsystem is obtained individually and this implies the possibility to transform only the controllable modes ($h^{[k]} = 0$) into normal form representation. The resulting complex normal form equations of the partly transformed pendulum system up to order O(2) state:

$$\dot{y} = \begin{bmatrix} A & 0 \\ 0 & C \end{bmatrix} y + \begin{pmatrix} f^{[2]}(y) \\ \mathfrak{g}^{[2]}(y) \end{pmatrix} + \begin{bmatrix} 0 \\ B \end{bmatrix} u. \quad (15)$$

3 Resonant coupling controller

The resonant coupling controller is based on the 1:2 coupling of the underactuated uncontrollable modes with the actuated controllable modes. Assuming $A = \operatorname{diag}\{-\mathrm{i}\omega, \mathrm{i}\omega\}$ and $C = \operatorname{diag}\{-\mathrm{i}\omega_{\mathrm{d}}, \mathrm{i}\omega_{\mathrm{d}}\}$ to represent both subsystems as well as

$$G = \begin{pmatrix} 0 \\ B \end{pmatrix},\; B = \begin{bmatrix} 1 & i \\ 1 & -i \end{bmatrix} \in \mathbb{C}^{2\times 2} \quad (16)$$

and

$$\nu(\xi,\eta)=\begin{pmatrix}0\\0\end{pmatrix},\ u=\begin{pmatrix}u_1\\u_2\end{pmatrix}, \tag{17}$$

the normal form of the controllable subspace ($k=2$) is identified as (suppressing the complex conjugate equation of $\dot{\bar{\eta}}$)

$$\dot{\eta}=-i\omega_d\eta+\mathfrak{g}^{(2,0)}_{1:2000}\xi^2+u_1+iu_2, \tag{18}$$

indicating the desirable form of the controlled subsystem. Only nonlinearities in the form of resonant coupling monomials ξ^2 are permitted in order to dissipate energy from the uncontrollable modes. Hence, the designed controller considers damping (k), coupling enforcement (e), and $\alpha^{[k]}$ to erase the non-normal form monomials:

$$u_{\dot{\eta}}(\xi,\eta)=u_1+iu_2=k\eta+ie\xi^2+\alpha^{[2]}(\xi,\eta). \tag{19}$$

Since (18) is the desirable form of the controllable subsystem one has to assure the physical system can be brought to such form. Thus, the original controllable subsystem in complex coordinates

$$\begin{aligned}\dot{z}_c=&-i\omega_d z_c+g^{(2,0)}_{1:2000}z_u^2+g^{(2,0)}_{1:0200}\bar{z}_u^2\\&+g^{(2,0)}_{1:1100}z_u\bar{z}_u+u_1+iu_2\end{aligned} \tag{20}$$

is modified by the control input (19) by use of the implicit function theorem. After choosing $\alpha^{[2]}$ to erase non-normal form monomials one derives the final form of the control input in complex states as:

$$u_{\dot{z}_c}(z_u,z_c)=\underbrace{kz_c}_{u_1}+\underbrace{iez_u^2-g^{(2,0)}_{1:0200}\bar{z}_u^2-g^{(2,0)}_{1:1100}z_u\bar{z}_u}_{iu_2}. \tag{21}$$

The controller in (21) is designed for the case of $\omega:\omega_d=1:2$ resonance coupling. Further details regarding the derivations are collected in [Rapp et al., 2011]. Expanding the controller design to spatial domain (1:1:2 coupling) incorporates 1:1 and 1:2 resonances respectively. In general 1:1 resonant coupling investigation reveals coupling monomials of order O(3) ([Nayfeh and Mook, 1979]). The normal form coordinates are extended to $y=\left(\xi_1,\bar{\xi}_1,\xi_2,\bar{\xi}_2,\eta,\bar{\eta}\right)^T$ in order to include two uncontrollable (deflection) modes and one controllable mode. Cubic nonlinearities with respect to 1:1 resonant coupling can be identified in a similar manner as the quadratic resonant terms for 1:2 resonance.

The aforementioned controller is implemented to control the underactuated system representing the hoisting device of a container crane (trolley, ropes, container). The control is applied to a general hoisting maneuver ($l_0\approx 9\text{m}, \dot{l}_{ref}=-0.1\text{m/s}, z_{u,0}=0, \dot{z}_{u,0}\neq 0, z_{c,0}=0, \dot{z}_{c,0}=0$). Figures 3 and 4 illustrate the simulation results of the load deflection as well as load trajectory without and with control of the hoisting process. The upper graph of Fig. 3 correlates with the left graph of Fig. 4 and vice versa. During constant hoisting, the deflection increases with decreasing rope length. In case of controlled hoisting by (21), the shape of the trajectory changes (Fig. 4, right) due to the input. As a result the deflection decreases as well as the rope length. The trolley position is not affected at all during the described hoisting maneuver. The details of the theoretical aspect of the reduced normal forms technique is presented in [Rapp et al., 2011].

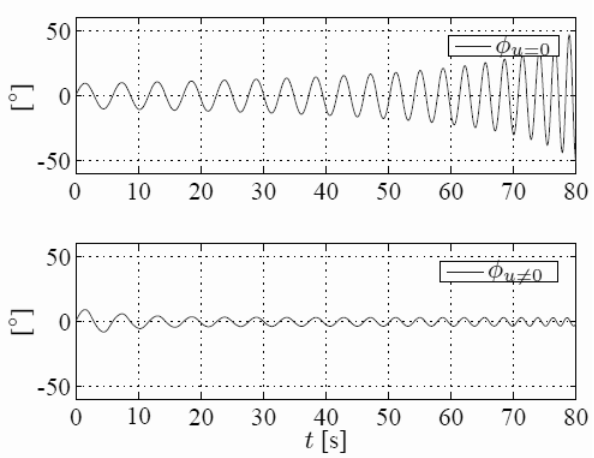

Figure 3. Load deflection without (top) and with (bottom) control.

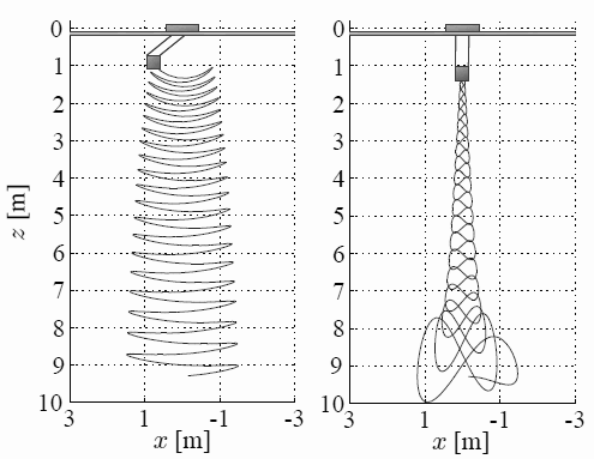

Figure 4. Load trajectory without (left) and with (right) control.

4 Experimental validation

The experimental validation of the reduced normal form control scheme is carried out at the container crane test stand at the laboratory of the Institute of Mechanics and Ocean Engineering, Hamburg University of Technology, Germany.

4.1 Container crane test stand

A sketch of the container crane test stand is shown in Fig. 5. Two parallel rails for the trolley are mounted directly at the ceiling to form the guiding track (hoisting height: 11m). The track is 15m long, which allows a traveling distance of about 13m. The rails consist of an aluminium box section (120mmx120mm) who carry one hardened steel rod with a diameter of 25mm on both sides to form a linear guidance. Eight roller elements are mounted on the trolley's edges which join into the steel rods and carry the weight of the trolley. The actual mass of the model container is 30kg, although, the stand is designed for a maximum payload of 150kg.

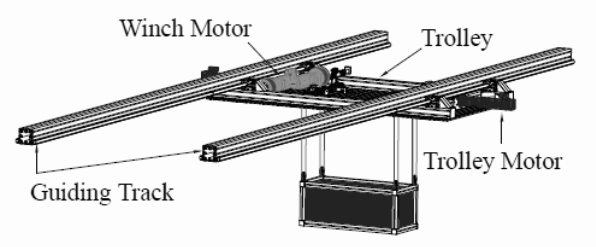

Figure 5. Sketch of the container crane test stand.

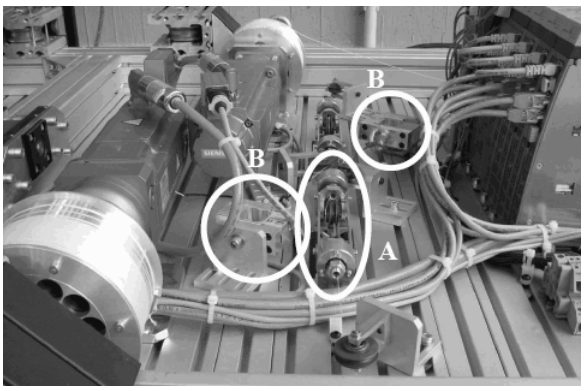

Figure 6. Trolley with winches and rope guidance.

The trolley, details are shown in Fig. 6, is driven by one controller-based synchronized Siemens 1FT7034 servo drive on each side to provide a momentum free driving force (maximum of 600N), which results in a maximum trolley acceleration of 2m/s^2 for a 30kg payload and a trolley mass of 270kg. The maximum trolley speed is 3m/s, compared to the maximum speed of a real trolley of about 4m/s. While real container cranes contain two winch motors to hoist the containers, the test stand holds four Siemens 1FT7044 servo drives to control each cable independently. The aluminium cable drums are mounted directly on the output shaft of the servo's planetary gearbox. On each top corner of the container a pulley is mounted, just like a real container spreader, hence, the loose end of the cable runs from the drum, passes two defector rolls of the cable guidance system (detail A of Fig. 6), continues to the container's pulley, gets deflected upwards, passes another pair of deflection rolls and is fixed at the force transducer (detail B). Using this kind of cable guidance, the kinematics of the model container are identical to the real container. The two inner deflection rolls handling the vertical parts of the cable are mounted on a common frame which is pivoted by roller bearings. This design forces the rolls to follow the cable to the side, when the container swings perpendicular to the trolley's track and prevents the cable from jumping off the roll at high hoisting speeds. The cables are synthetic Dyneema cables of 1mm diameter, which are normally used for kites. The stiffness of the pre-stretched cable equals the stiffness of a steel cable, but the damping in longitudinal direction is much better. This is an important benefit compared to steel cables, as the frequencies of the first longitudinal and bending modes of the reeled out cable is in the same region as the frequency of the load oscillations, so filtering of these disturbances measured by the force transducers is not possible. The drawback in using Dyneema cables is in the higher amount of servicing the test stand, as the cables have to be replaced more often for safety reasons.

The maximum hoisting speed is 3m/s, which is the same speed real cranes are operated at. The winches and the trolley are controlled by a Siemens SIMOTION D435 controller, combined with Siemens SINAMICS S120 power electronics components. For flexibility reasons, controllers, the processing of the measurement data and the human-machine-interface is set up using National Instrument's LabVIEW, running on a PC based real-time controller. On the basis of this concept the controllers are developed in three steps: design and simulation using MATLAB, translation of MATLAB code to C-code and building a DLL file, integration of the DLL into the LabVIEW environment using a designated data interface. The loop rate of the LabVIEW controller is 200Hz, which is limited by the Profibus. Via Profibus network the force measurements, rope length and rope velocities of each hoist, plus the position and velocity of the trolley are transfered to the LabVIEW controller, routing feedback signals to the anti-swing controllers. Additionally, each axis' set point is sent to the SIMOTION controller. There are no container position measurements to be directed to the controller, because the camera systems on real cranes

are not capable of tracking the container position at the test stand's scale. The only camera that is used for offline validation measurements of the load sway estimator described in the following section. Therefor a 100Hz C-MOS camera is used, which captures the scene within the plane of trolley motion and gravitational axis at a resolution of 640x480 pixel. For getting better contrast four LED–illuminated balls are attached to one side of the container. These bright markers are sensed by the camera, whereas no further objects in the lab are sensed and no special illumination of the scene is needed. After extraction of the coordinates of the four bright spots, the planar position of the container is calculated using an inverse nonlinear camera model calibrated by the method of [Lenz, 1987]. The resulting position data is collected to be compared with estimated position data for validation purposes.

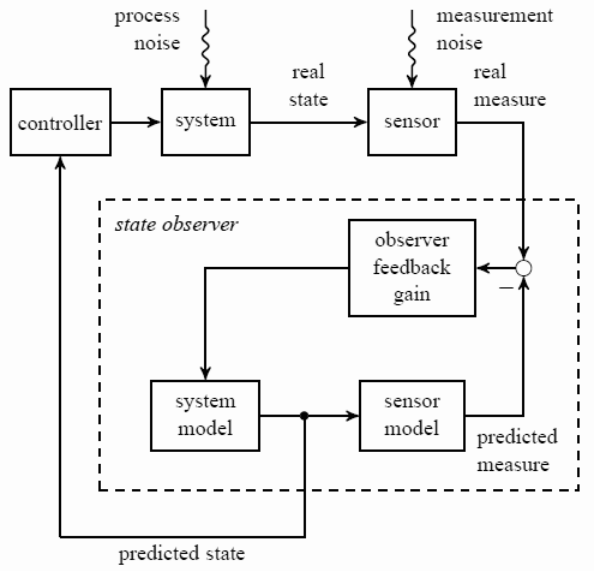

Figure 7. Control system with observer.

4.2 Load sway estimation

The test stand only holds a limited number of sensors to acquire information about the system's behavior. Namely, the rope forces F_i $(i = 1 \dots 4)$ are measured but no data about the deflection of the container is available. In order to evaluate the deflection as well as the rate of change of deflection of the container $x_u = (\phi, \dot{\phi})^T$ with respect to the constant trolley position a state observer is employed. Figure 7 demonstrates a general control system, which contains an observer to predict the states of the system. On the basis of the predicted states the control can be evaluated and applied to the real system. The sensor takes data samples, which are compared with predicted samples as part of the observer. Based on the noise variances and the system state the observer feedback gain is calculated to scale the discrepancy between predicted and measured sensor data. The scaled signal is fed back to the system model to adjust the state variables depending on the discrepancy and the state as a correction step.

The choice of observer outline is dominated by the characteristics of the system and sensor model. Both are described in detail by [Theis, 2010]. The author points out that fully nonlinear models are required to properly evaluate the response. Thus, an Unscented Kalman Filter (UKF) is chosen for implementation in order to meet these requirements (see [Julier et al., 1995] and [Theis, 2010]). The UKF is based on an unscented transformation introduced by [Julier, 2002], which approximates the nonlinear system and sensor equations by means of stochastic processes. As a result the predicted states are the mean values of deflection $\hat{\phi}$ and rate of change of deflection $\dot{\hat{\phi}}$ together with its standard deviations $(\sigma_{\hat{\phi}}, \sigma_{\dot{\hat{\phi}}})$. This technique provides benefits in terms of low installation cost for sensors, robustness and real-time capability. Being able to acquired zero-delay state information clearly enhances the possibility to assign system control. Some observation results are displayed by Fig. 8 along with the validation data from camera measurements. The predicted states correlate with the camera measurements, hence, the results of the control are given in terms of the predicted deflection state $\hat{\phi}$.

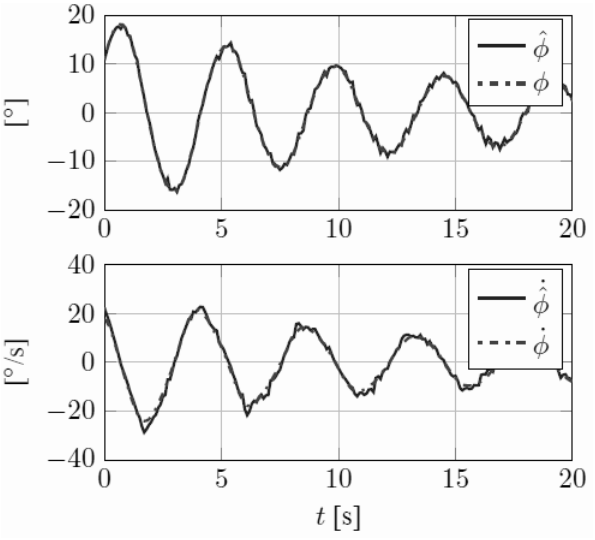

Figure 8. Validation of UKF with camera.

4.3 Results

The response of the real system with respect to a control law based on 1:2 internal resonance is investigated. As a first step, a simplified resonance coupling control scheme is employed. The hoisting manipulation control from [Bockstedte and Kreuzer, 2005] imposes a spring-mass-dashpot behavior on the con-

trollable mode $x_c = (l - l_0, \dot{l} - \dot{l}_{ref})^T$ of the elastic pendulum. The spring constant c is tuned to meet the resonance condition $\omega_d = \sqrt{c} = 2\omega$. The dashpot dissipates energy of the controllable mode, which is transfered through the resonance coupling and originates from the load deflection.

Fig. 9 contains the deflection (uncontrollable mode, upper plot) as well as the elongation of the pendulum's rope (controllable mode, lower plot). The controller starts at an initial deflection of approximately 10°. Instantaneously, $(l - l_0)$ increases up to the point when the influence of the dashpot dominates its response ($\approx$ 6s). The frequency matches ω_d, which is by definition twice the load swing frequency. Due to the controlled elongation of the rope, the deflection is decreased by resonant coupling of both modes. Within 20s the absolute deflection is reduced from almost 20° to less than 10°.

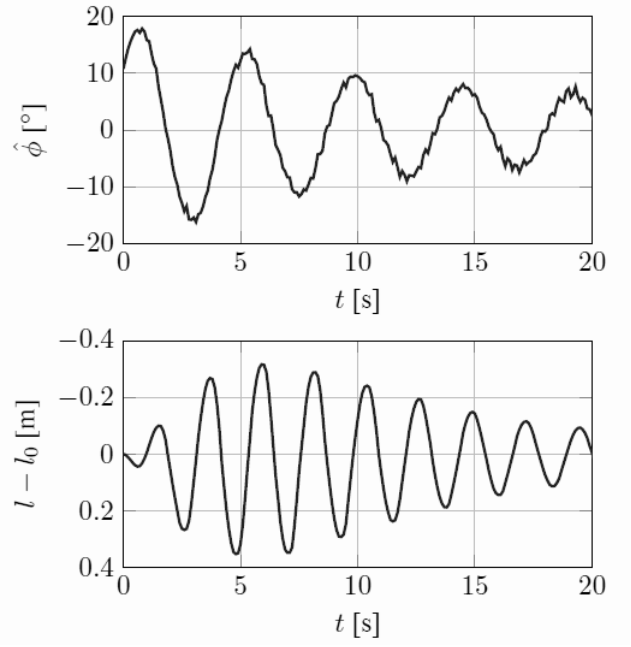

Figure 9. Control without hoisting: deflection and elongation.

So far, the system has been fixed at a reference length l_0 of the controllable mode. Next, a hoisting process is examined. The reference length of the rope states $l_{ref}(t) = \dot{l}_{ref}t + l_0$. Two cases are created: an initially deflected pendulum is hoisted without (1) and with (2) hoisting manipulation. The configuration parameters of the test cases are set as $l_0 = 7$m, $\dot{l}_{ref} = -0.2$m/s, $l_{min} = 4$m.

The first case is depicted in Fig. 10. It can be found to increase the deflection (upper plot) due to constant hoisting without manipulation (lower plot). During this process, the length continuously decreases whereas the oscillation frequency increases until the hoisting is stopped at minimum length l_{min}. Employing the resonance coupling control scheme from [Bockstedte and Kreuzer, 2005] shows superior behavior, see Fig. 11. The deflection (upper plot) is dramatically reduced during the hoisting process. The controller manipulates the hoisting velocity $\dot{l}$ with respect to the current states of the system. It increases the hoisting at maximum deflection whereas the velocity decreases around the equilibrium position, leading to the depicted trajectory of the lower plot in Fig. 11.

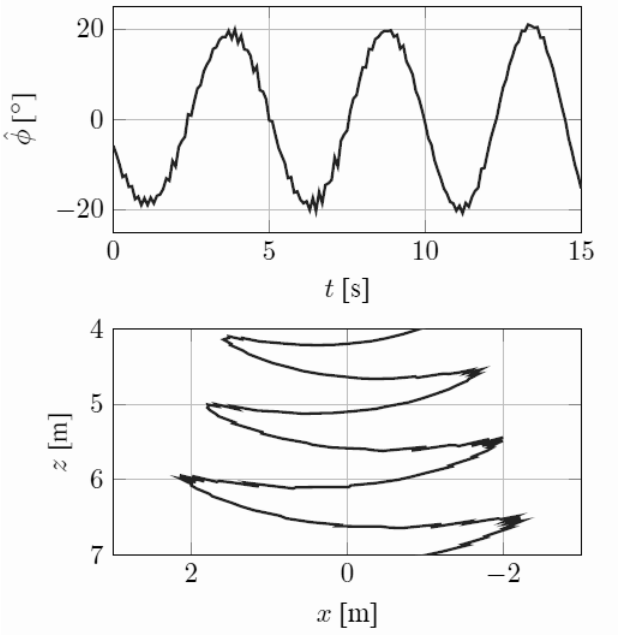

Figure 10. Hoisting without control: deflection and trajectory.

As mentioned, the control law follows [Bockstedte and Kreuzer, 2005]. A comparison of the employed control law to (21) shows some correlation. The spring-mass-dashpot (smd) formulation contains only $u_{\dot{z}_c,\text{smd}} = u_1 = kz_c$ but does not contain the coupling disturbance rejection $\alpha^{[2]}$ nor coupling enhancement e. This leads to the fact that the implemented control scheme at the container crane test stand so far only offers limited insight in the effectiveness of the resonant coupling control. Nevertheless, Fig. 12 emphasizes through simulation results the possible improvement of the resonant coupling control over the spring-mass-dashpot control law. Although the control input is reduced (lower plot), the deflection is reduced quickly. Whereas the control law from [Bockstedte and Kreuzer, 2005] only slowly decreases the oscillations.

5 Conclusion

The reduced normal form is much more transparent than the classical normal form derivation. It is successfully applied to a general autonomous nonlinear control system with multiple inputs ([Krener et al., 2001]

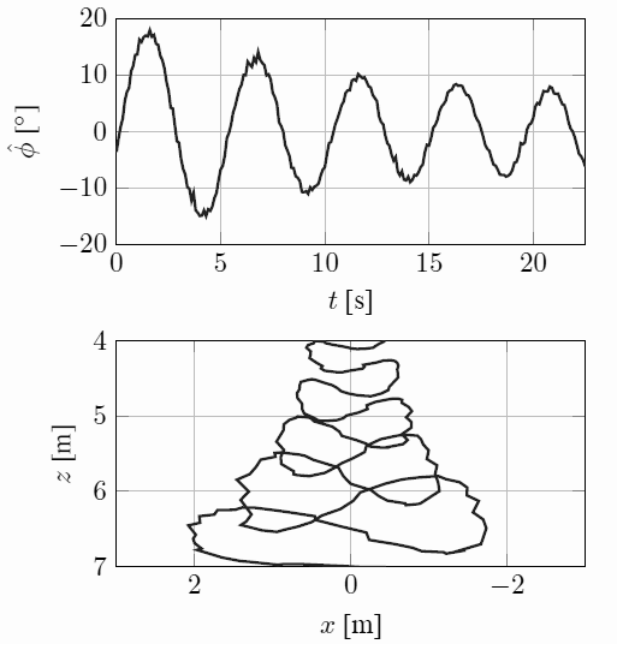

Figure 11. Hoisting with control: deflection and trajectory.

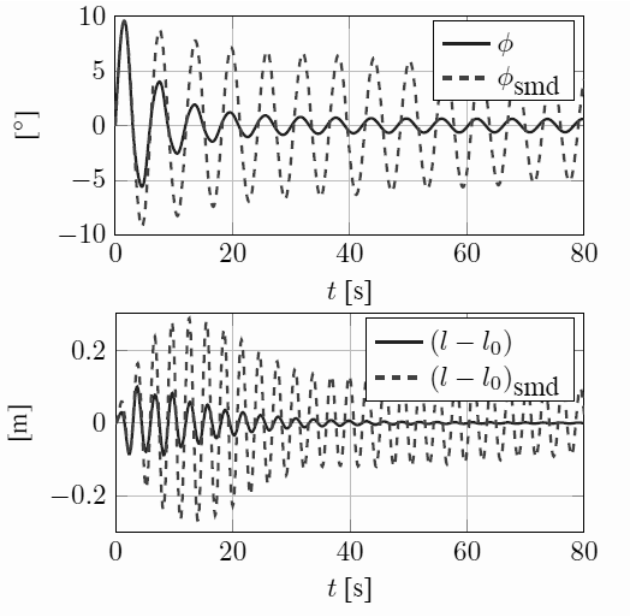

Figure 12. Resonant coupling control vs. spring-mass-dashpot control: deflection and elongation.

uses a single input). Energy dissipation from the underactuated system is directly revealed, thus, the reduced normal form identifies the coupling monomials of the controllable subsystem of a general nonlinear control system. Using this knowledge the designed controller successfully dissipates energy from the uncontrollable subsystem by 1:2 resonant coupling. The results are validated at the container crane test stand at the Institute of Mechanics and Ocean Engineering. The authors are aware of the fact that, although, the cost of calculation of the reduced normal form is decreased, the presented method is only valid for a limited range of problems due to nature of normal forms. Hence, resonant coupling control is effectively applied to the container crane test stand and will shortly be extended to the control law (21) for further improvement of load swing reduction.

Acknowledgements

This research project is part of the research training group *Ports for Container Ships of Future Generations* funded by the *German Research Foundation (DFG)*. The experimental setup was funded by the *DFG* and the *Hamburg University of Technology*. We thank the *Siemens AG* for supporting the project, especially Mr. Thomas Breuer from the Industry Automation & Drive Technologies Division.

References

Abdel-Rahman, E.M., Nayfeh, A.H., and Masoud, Z.N. (2003) Dynamics and control of cranes: a review. *J. Vib. Control*, **9**, pp. 863–908.

Arnold, V.I. (1983) *Geometric Methods in the Theory of Ordinary Differential Equations*. Springer-Verlag, New York.

Bockstedte, A., and Kreuzer, E. (2005) Crane dynamics with modulated hoisting. *Proc. Appl. Math. Mech.* **5**, pp. 83–84.

Julier, S.J., Uhlmann, J.K., and Durrant-Whyte, H.F. (1995) A new approach for filtering nonlinear systems. *Proc IEEE American Control Conference*, pp. 1628–1632.

Julier, S. (2002) The scaled unscented transformation. *Proc IEEE American Control Conference*, pp. 4555–4559.

Khajepour, A., and Golnaraghi, M.F. (1994) Internal resonance controller design using normal forms. *Nonlinear and Stochastic Dynamics*, **DE 78/AMD 192**, pp. 143–150.

Khajepour, A., Golnaraghi, M.F., and Morris, K.A. (1997) Modal coupling controller design using normal form method, part II: control. *J. Sound Vib.* **205**, pp. 671-688.

Krener, A.J., and Kang, W. (1990) Extended normal forms of quadratic systems. *Proc 29th IEEE Conf on Decision and Control*, **1**, pp. 1223-1229.

Krener, A.J., Kang, W., and Chang, D.E. (2001) Normal forms of linearly uncontrollable nonlinear control systems with a single input. *Proc IFAC*

Symposium on Nonlinear Control Systems.

Lenz, R. (1987) Linsenfehlerkorrigierte eichung von halbleiterkameras mit standardobjektiven fr hochgenaue 3D-messungen in echtzeit. *Informatik Fachberichte Bd.* **149**, pp. 212–216.

Nayfeh, A.H., and Mook, D.T. (1979) *Nonlinear Oscillations*. Wiley-Interscience Publication, New York.

Rapp, C., Kreuzer, E., and Namachchivaya, N.S. (2011) *Reduced Normal Forms for Nonlinear Control of Underactuated Hoisting Systems*. Published online in Arch Appl Mech. DOI 10.1007/s00419-011-0557-5.

Talwar, S. and Namachchivaya, N.S. (1992) Control of chaotic systems: application to the Lorenz equation. *Nonlinear Vibrations*, **DE 50/AMD 144**, pp. 47–58.

Theis, J. (2010) *Beobachterentwurf für einen räumlich pendelnden Körper mit steuerbarer Aufhängung (in German)*. Bachelor's thesis, Hamburg University of Technology.